

## TENSILE SIMULATION OF 6061 ALUMINUM ALLOY

Received – Priljeno: 2023-05-08

Accepted – Prihvaćeno: 2023-08-29

Original Scientific Paper – Izvorni znanstveni rad

The quasi-static tensile simulation was carried out on the 6061 aluminum alloy round bar specimen, and the tensile specimen model was drawn. Three sets of simulation with uniaxial tensile velocity of  $10\text{ s}^{-1}$ ,  $15\text{ s}^{-1}$  and  $20\text{ s}^{-1}$  were set at normal temperature, and the numerical simulation of the tensile process was carried out by using ABAQUS software. The experimental data were imported into the model, and the relevant parameters such as damage model were set. The derived simulation results are in good agreement with the experimental results, indicating that the established simulation model can simulate the uniaxial tensile behavior of 6061 aluminum alloy well.

**Keywords:** 6061 aluminum alloy; static drawing; mises stress; stress-strain curves; numerical simulation

### INTRODUCTION

6061 aluminum alloy is a high quality aluminum alloy product produced by heat treatment and predrawing process[1]. Its chemical composition is shown in Table 1. Because of its good formability, weldability, machinability, at the same time has moderate strength, after annealing can still maintain good operation, become the metallurgical industry commonly used metal materials[2]. 6061 aluminum alloy is mainly used for high-load parts and component materials, such as skeleton parts on aircraft, skin, space rocket storage box, etc.

Table 1 **Chemical composition of 6061 aluminum alloy/wt. %**

Si	0,4~0,8	Cr	0,04~0,35
Fe	0,7	Zn	0,25
Cu	0,15~0,4	Ti	0,15
Mn	0,15	Al	Others
Mg	0,8~1,2		

As a kind of ductile material, the uniaxial stress-strain relationship of 6061 aluminum alloy is the basic physical relationship for structural analysis and engineering design by using continuum mechanics method, which plays a key role in the design and safety evaluation of engineering samples[3]. After necking occurs in the iso-straight specimens, the load gradually decreases[4], and the material element in the necking zone is in the strengthening stage of complex deformation. In this paper, the real stress-strain relationship after necking is obtained by traditional uniaxial tensile test, and the finite element model of 6061 aluminum alloy bar is established by using ABAQUS finite element software, whose style parameters are shown in Figure 1. The stress-strain relationship of ductile metal of 6061 alu-

minum alloy was obtained by the traditional uniaxial tensile simulation using the straight round bar specimen. Finally, the simulated stress-strain relationship of ductile metal material of 6061 aluminum alloy was compared with the real stress-strain relationship obtained from traditional uniaxial tensile test, and the established model was verified to be suitable for predicting the tensile behavior of 6061 aluminum alloy.

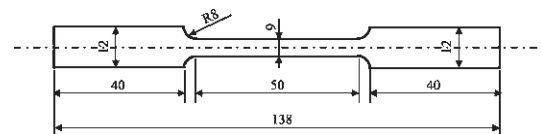


Figure 1 6061 aluminum alloy bar sample

### ESTABLISHMENT OF FINITE ELEMENT MODEL

ABAQUS finite element simulation software was used to draw bar material, and 6061 aluminum alloy material properties were introduced. The density was  $2700\text{ kg/m}^3$ , elastic modulus was 50 GPa and Poisson's ratio was 0,33. The effective stress-strain relationship of 6061 aluminum alloy material should be input in the plastic section (Figure 2), and the value of flexible damage is shown in Table 2.

The three-dimensional model of uniaxial tensile simulation sample of 6061 aluminum alloy was established according to the sample size in Figure 1, as shown in Figure 3(a). C3D8R was used for the grid unit, and the global seed distribution and medial axis algorithm were used for grid division, as shown in Figure 3(b). A reference point RP-1 was established at the top end of the model and coupled with the top surface, as shown in Figure 3(c), to facilitate subsequent loading of boundary conditions. In order to simulate the stretching process, completely fixed boundary conditions were applied to one end of the model, and different constant stretching speeds were applied to the other end along

Z. C. Fu, Z. L. Zhao, F. Wang, T. K. Li, Y. Guo, H. C. Ji (E-mail: jihongchao@ncst.edu.cn) College of Mechanical Engineering, North China University of Science and Technology, Hebei, Tangshan, China.

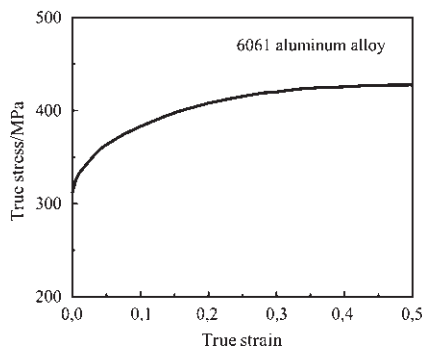


Figure 2 Stress-strain curve of 6061 aluminum alloy

Table 2 Values of flexible damage

Serial number	Fracture strain	Triaxial stress	Strain ratio
1	1	0	0,9
2	0,5	0,4	0,9

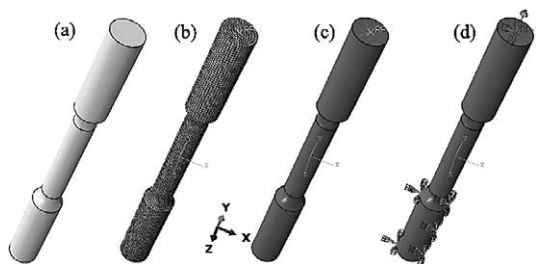


Figure 3 Construction process of tensile finite element model (a) three-dimensional sample model (b) mesh division (c) coupling setting (d) boundary condition setting

the negative Y-axis. The six degrees of freedom on the lower surface of the bar model are completely fixed, and the tensile velocity along the negative Y-axis is applied to the reference point, as shown in Figure 3(d).

### SIMULATION PROCESS

In order to illustrate the simulation process and model effectiveness, the tensile speed of  $10\text{ s}^{-1}$ ,  $15\text{ s}^{-1}$  and  $20\text{ s}^{-1}$  were selected as three working conditions to demonstrate and illustrate.

Figure 4 shows the Mises stress change in  $10\text{ s}^{-1}$  uniaxial tensile simulation at normal temperature. From Figure 4(a), it can be seen that only the middle part and the fillet transition and the upper part of the sample are stressed at the beginning of tensile. The Mises stress at the upper and middle ends increased significantly when the Mises was stretched to the point of necking (Figure 4(b)). When the specimen was about to be broken (Figure 4(c)), the Mises stress region was mainly concentrated at the fracture and the upper end.

Figure 5 shows the comparison of true stress-strain curves of  $10\text{ s}^{-1}$  uniaxial tensile simulation and experiment. The simulation curve is taken from one of the units at the fracture. As can be seen from Figure 5, the two curves fit well, indicating that the established  $10\text{ s}^{-1}$  uniaxial tensile simulation model can simulate the real tensile experiment well.

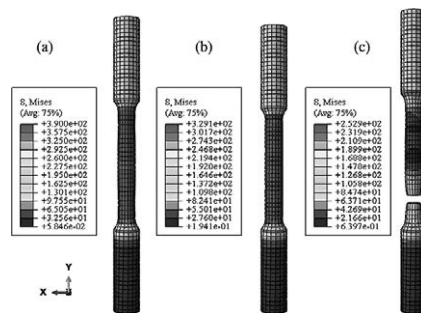


Figure 4  $10\text{ s}^{-1}$  uniaxial tensile simulation of Mises stress at normal temperature (a) when the specimen begins to draw (b) during the tensile process (c) when the specimen breaks

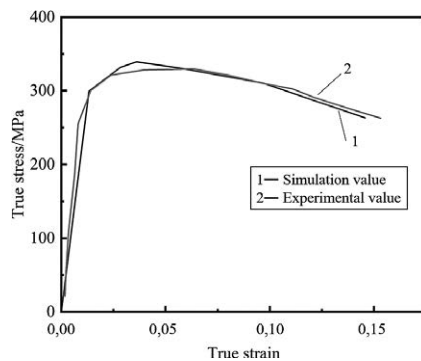


Figure 5 Comparison of experimental and simulated stress-strain curves at  $10\text{ s}^{-1}$

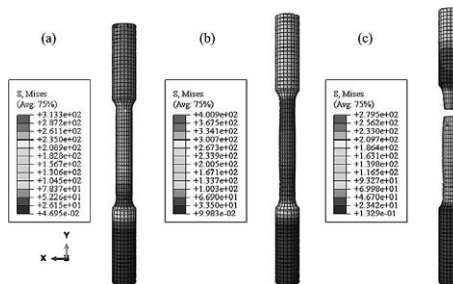
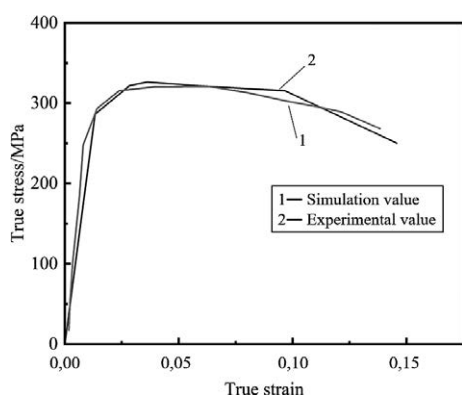


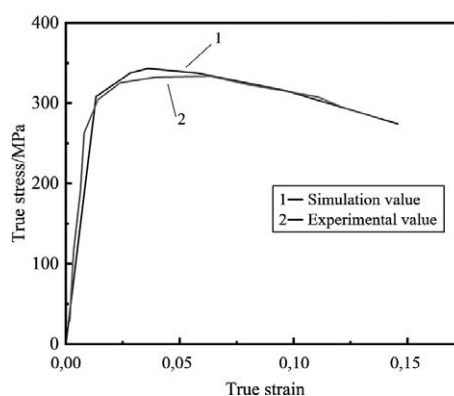
Figure 6 Uniaxial tensile simulation of  $15\text{ s}^{-1}$  Mises stress at normal temperature (a) when the specimen begins to draw (b) during the tensile process (c) when the specimen breaks

Figure 6 shows the change of Mises stress in the uniaxial tensile simulation of  $15\text{ s}^{-1}$  at normal temperature. As can be seen from Figure 6(a), only the middle part of the sample is subjected to a large tensile force at the beginning of stretching, and the lower part of the middle part has the largest force. When the Mises stress in the middle part was increased significantly and the Mises stress in the upper part was increased when the elongation reached the threshold of necking (Figure 6(b)). When the specimen was about to break (Figure 6(c)), the Mises stress region was mainly concentrated in the middle part.

Figure 7 shows the comparison of true stress-strain curves between simulation and experimental uniaxial tensile tests in  $15\text{ s}^{-1}$ . The simulation curve is taken from one of the elements at the fracture. As can be seen from Figure 7, the simulation data is larger than the experimental data at the maximum stress, but in general the two curves are in good agreement, indicating that the



**Figure 7** Comparison of experimental and simulated stress-strain curves under  $15 \text{ s}^{-1}$



**Figure 9** Comparison of experimental and simulated stress-strain curves under  $20 \text{ s}^{-1}$

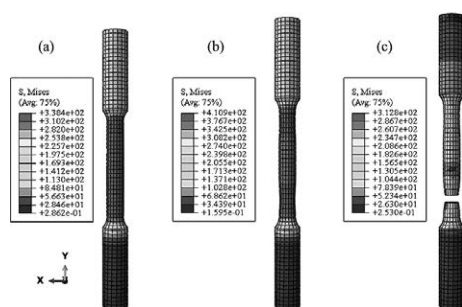


**Figure 8** Uniaxial tensile simulation of  $20 \text{ s}^{-1}$  Mises stress change at normal temperature (a) when the specimen begins to draw (b) during the tensile process (c) when the specimen breaks

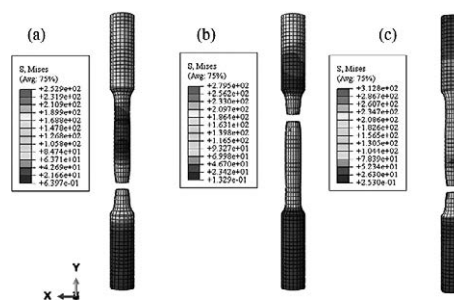


**Figure 10** Changes of simulated Mises stress in 6061 aluminum alloy bars at different uniaxial tensile speeds

established  $15 \text{ s}^{-1}$  uniaxial tensile simulation model can simulate the real tensile experiment well.

Figure 8 shows the Mises stress change under normal temperature in  $20 \text{ s}^{-1}$  uniaxial tensile simulation. As can be seen from Figure 8(a), at the beginning of tensile, almost only the middle and upper sections of the sample were stressed. The Mises stress at the upper and middle ends increased significantly when the Mises was stretched to the point of necking (Figure 8(b)). When the specimen was about to break (Figure 8(c)), the Mises stress was mainly concentrated in the fracture and the middle section.

Figure 9 shows the comparison between simulation and experimental stress-strain curves of uniaxial tensile in  $20 \text{ s}^{-1}$ . The simulation curve is taken from one of the units at the fracture. As can be seen from Figure 9, the simulation data at the last and last sections are smaller than the experimental data, but generally the two curves are in good agreement, indicating that the established  $20 \text{ s}^{-1}$  uniaxial tensile simulation model can simulate the real tensile experiment well.

Figure 10 shows the simulation stress changes of 6061 aluminum alloy bar at  $10 \text{ s}^{-1}$ ,  $15 \text{ s}^{-1}$  and  $20 \text{ s}^{-1}$  respectively at normal temperature. It can be seen that the faster the tensile speed is, the greater the stress will be.

## CONCLUSION

Through the above experiment and simulation analysis, the following conclusions can be drawn:

1) Stress increases with the increase of tensile rate at room temperature;

2) Through the above experiments and simulation analysis, it can be concluded that the stress-strain curves simulated by ABAQUS are in good agreement, indicating that ABAQUS simulation has high accuracy in predicting fracture displacement and stress-strain, and the established model can be used to predict the tensile behavior of 6061 aluminum alloy.

## Acknowledgments

This work is supported by the Tangshan Talent Foundation Innovation Team (20130204D) and funded by Key research and development plan of Tangshan science and technology (22281802Z).

## REFERENCES

- [1] X S Shi. Damage and fracture behavior of 2024 aluminum alloy sheet in hot deformation process and modeling analysis[D]. Wuhan: Huazhong University of Science and Technology, 2016.
- [2] X H Peng, Y M Yang, Y Z Chen, et al. Study on Tensile Failure and Its Mechanism of LY12 Aluminum Alloy under High Temperature Rise [J]. Chinese Journal of Solid Mechanics (2005) 1, 72-76.
- [3] J Liu, R L Shen, L H Zhan, et al. Study on Forming Limit Diagram of 2A12 Duralumin Alloy Sheet in Hot Drawing [J]. Forging & Stamping Technology (2018) 43, 7.
- [4] M Karoglou, A Moropoulou, Z B Maroulis, et al. Water Sorption Isotherms of Some Building Materials [J]. Drying Technology (2005) 23, 289-303.

**Note:** The responsible translator for English language is H. C. Ji-North China University of Science and Technology, China